Pacific Northwest
NATIONAL LABORATORY

PNNL-31720

Radiation Stability of MOF Engineered Particles

July 2021

1 Praveen K. Thallapally
2 Alexander J. Robinson
3 Jarrod V. Crum
4 Mark K. Murphy
5 Matthew R. Lish (Flibe Energy)

U.S. DEPARTMENT OF ENERGY

Prepared for the U.S. Department of Energy
under Contract DE-AC05-76RL01830

DISCLAIMER

PACIFIC NORTHWEST NATIONAL LABORATORY
operated by
BATTELLE
for the
UNITED STATES DEPARTMENT OF ENERGY
under Contract DE-AC05-76RL01830

Printed in the United States of America

Available to DOE and DOE contractors from the
Office of Scientific and Technical Information,
P.O. Box 62, Oak Ridge, TN 37831-0062;
ph: (865) 576-8401
fax: (865) 576-5728
email: reports@adonis.osti.gov

Available to the public from the National Technical Information Service
5301 Shawnee Rd., Alexandria, VA 22312
ph: (800) 553-NTIS (6847)
email: orders@ntis.gov <https://www.ntis.gov/about>
Online ordering: http://www.ntis.gov

PNNL-31720

Radiation Stability of MOF Engineered Particles

July 2021

1 Praveen K. Thallapally
2 Alexander J. Robinson
3 Jarrod V. Crum
4 Mark K. Murphy
5 Matthew R. Lish (Flibe Energy)

Prepared for
the U.S. Department of Energy
under Contract DE-AC05-76RL01830

Pacific Northwest National Laboratory
Richland, Washington 99354

Abstract

Pacific Northwest National Laboratory (PNNL), in collaboration with Flibe Energy, demonstrated the fabrication of metal organic frameworks (MOFs) into engineered beads to manage off-gases released from molten salt reactors. Based on the commercial availability and ease to synthesis at scale, PNNL down-selected two MOF sorbents known as CuBTC and UiO-67. The sorbents were synthesized, characterized, and fabricated into mechanically robust engineered beads (composites) using wet granulation method using a polymer as a binder. Further, MOF powders and mechanically robust composites were exposed to gamma radiation using a Co-60 source and the irradiated MOFs were characterized to demonstrate the structural stability. Among the two MOF sorbents identified, the CuBTC MOF was shown to be very promising for noble gas management at low temperature (193 K) compared to UiO-67 MOF. The high adsorption capacity of the synthesized composites was correlated to the high specific surface area and pore volume of the CuBTC MOF. Both MOFs retain structural integrity and long-range order even after exposure to 1000 kGy of radiation.

Summary

Pacific Northwest National Laboratory (PNNL), in collaboration with Flibe Energy, demonstrated the fabrication of metal organic frameworks (MOFs) into engineered beads to manage off-gases released from molten salt reactors. Based on the commercial availability and ease to synthesis at scale, PNNL down-selected two MOF sorbents known as CuBTC and UiO-67. The sorbents were synthesized, characterized, and fabricated into mechanically robust engineered beads (composites) using wet granulation method using a polymer as a binder. Further, MOF powders and mechanically robust composites were exposed to gamma radiation using a Co-60 source and the irradiated MOFs were characterized to demonstrate the structural stability. Among the two MOF sorbents identified, the CuBTC MOF was shown to be very promising for noble gas management at low temperature (193 K) compared to UiO-67 MOF. The high adsorption capacity of the synthesized composites was correlated to the high specific surface area and pore volume of the CuBTC MOF. Both MOFs retain structural integrity and long-range order even after exposure to 1000 kGy of radiation.

This report completes the two milestones entitled “Synthesis, characterization of MOF engineered forms and radiation stability” (M4SB-19PN0201072) and “Characterize the post irradiation of MOFs” (M4SB-19PN0201073).

Acknowledgments

This effort was funded by the DOE Office of Nuclear Energy GAIN Voucher. We thank Kimberly Gray and Stephen Kung (DOE) for support. Patricia Paviet, John Vienna, Brian Riley, Josef (Pepa) Matyas, Ali Zbib and Mark Nutt (PNNL) for helpful discussion and thoughts. We also thank Dr. Matthew Lish at Flibe Energy for helpful discussion and support.

Acronyms and Abbreviations

BET	Brunauer-Emmett-Teller
DOE	U.S. Department of Energy
GAIN	Gateway for Accelerated Innovation in Nuclear
HKUST-1	Hong Kong University of Science and Technology
LFTR	liquid fluoride thorium reactor
NE	Office of Nuclear Energy
PAN	polyacrylonitrile
PMMA	poly methyl methacrylate
PNNL	Pacific Northwest National Laboratory
PXRD	powder X-ray diffraction
RT	room temperature
SEM	scanning electron microscopy
UiO	University of Oslo

Contents

Figures

Tables

1.0 Introduction

Recently, crystalline microporous materials – including metal organic frameworks (MOFs), porous organic cages, covalent organic frameworks, and zeolites – were demonstrated to separate xenon and krypton at near room temperature.[1, 2] As part of the U.S. Department of Energy (DOE) Office of Nuclear Energy's Material Recovery and Waste Form Development Campaign, Pacific Northwest National Laboratory (PNNL) extensively worked on these materials to demonstrate the selective removal of Xe and Kr from a simulated composition relevant to nuclear reprocessing plants[3, 4]. In particular, MOFs have shown to be a very promising class of materials for selective removal of Xe and Kr because the pore size, shape, and specific surface area can be manipulated with the choice of organic building blocks and metal nodes. Among all the materials evaluated, it was found that materials with small pore sizes, i.e., just enough to accommodate a single Xe atom, would be ideal for separation; the same was true for Kr.[5]

We have demonstrated the two-column approach using a MOF where bed 1 selectively removes Xe at room temperature from a gas mixture consisting of 1300 ppm Xe, 130 ppm Kr, 400 ppm CO2, 0.9% Ar, 78.2% N2, and 21% O2. The off gas mixture (without Xe) exiting bed 1 was passed through bed 2, containing same MOF material at room temperature, to remove Kr.[6] The selectivity of the MOF in both bed 1 and bed 2 was calculated and found to be the best among the materials tested for room-temperature application. For example, selectivity of Xe toward other gases in bed 1 was found to be 14 (Kr), 3 (CO2), 209 (N2), 210 (Ar), and 206 (O2). Similarly, selectivity of Kr in bed 2 was found to be 0.3 (CO2), 9.9 (N2), 9.3 (Ar), and 9.3 (O2). Further, the Xe and Kr adsorption capacity was not affected even with 48% of relative humidity.

Based on the two-column approach, economic analysis was performed in comparison with cryogenic separation and suggested our room-temperature method shows significant cost reduction. The two-column approach is important because all the radioactive Xe has decayed away in about 1 month (in bed 1). The remaining, non-radioactive xenon is quite valuable, with many commercial applications in lighting, medicine, nuclear technology, and spacecraft propulsion.[7]

Though MOFs have shown promise for noble gas separation, limited or no efforts were found in the literature on the use of MOFs to manage noble gases released from molten salt reactors (liquid fluoride thorium reactor, LFTR). As part of the DOE Office of Nuclear Energy (NE) Gateway for Accelerated Innovation in Nuclear (GAIN) Voucher, PNNL, in collaboration with Flibe Energy, is evaluating MOFs to separate noble gases released from LFTR fuel. Due to national security concerns, the noble gases released from the LFTR fuel must be captured using delay beds to decay short- and long-lived fission gases. Current technology for noble gas capture relies on activated carbon to delay the flow of noble gases through an adsorber (carbon) bed.[8] This approach requires very large adsorber beds (due to the lower capacity) to handle the noble gas stream from a utility class power reactor, which significantly increases the footprint (noble gas management system). This increase in footprint brings associated increases in cost, construction time, and operations and maintenance. Further, in activated charcoal systems, the Xe is always mixed with Kr-85 because of the poor selectivity of carbon, having about a 10-year half-life, rendering the Xe unusable. Further, the size of these adsorber beds is prohibitive for some novel applications of LFTR technology. For example, it has been estimated that a 1100 MW boiling water reactor requires –four to five charcoal beds with 6- to 9-ft-diameter, 50-ft-long delay beds[9] followed by series of charcoal beds to separate non-volatile noble gases such as Xe and Ar, which have commercial value (Figure 1).[8] Further, it has been

documented that the use of charcoal might result in bed fires due to the presence of oxygen and heat produced as a result radioactive decay. On the other hand, MOFs with higher specific surface areas, capacities, and selectivities would require noble gas delay beds to be much smaller, more compact, and more modular in design.

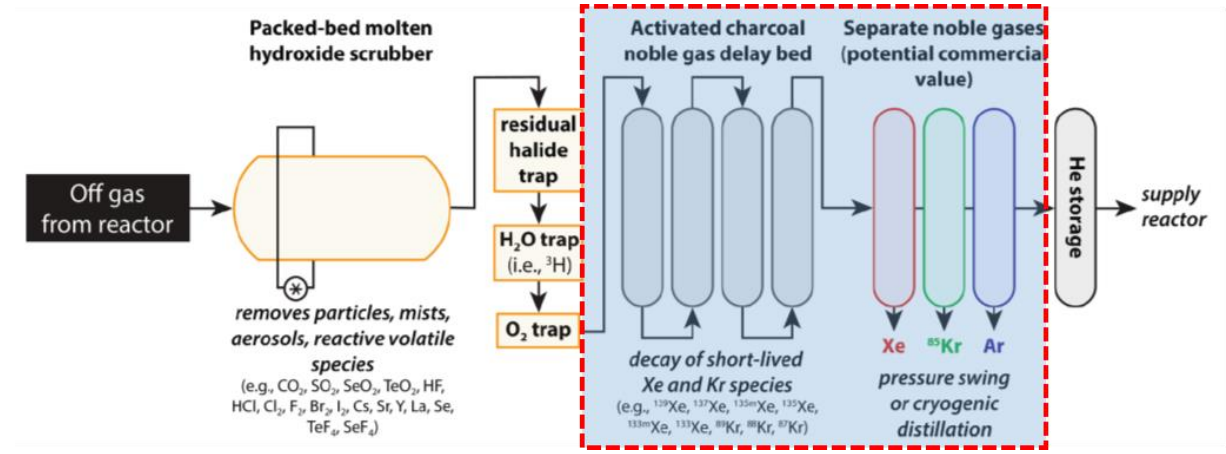

Figure 1. Schematic diagram of off-gas management system for molten salt reactors. The highlighted box shows the activated charcoal delay beds for short-lived noble gases followed by pressure swing adsorption to separation noble gases. Taken directly from reference 8.

Given the large body of MOF structures, we have selected CuBTC [copper-based MOF, also known as HKUST-1 (**H**ong **K**ong **U**niversity of **S**cience and **T**echnology)] as a potential sorbent because of its commercial availability, high specific surface area, and pore volume.[10-12] Along with the CuBTC MOF, PNNL evaluated the UiO-67 (**U**ni**O**slo) MOF and three commercially available activated carbon materials for comparison (Alamo water carbon, Yakima carbon, and NUCON carbon). All three carbon materials appear to be of uniform size with particle sizes ranging from 200 µm to more than 1000 µm and used without any further modification.

The CuBTC MOF is an open framework structure with a chemical formula of $Cu_3(BTC)_2$ $(H_2O)_n$, where BTC indicates 1,3,5-benzene tricarboxylate (Figure 2). The CuBTC forms face-centered cubic crystals that contain interconnected cavities that are 1.1, 1.3, and 0.5 nm. The UIO-67 MOF has a cubic three dimensional framework and is known to possess high radiation and chemical stability in aqueous solutions because each zirconium metal is connected to 12 organic building blocks to create $Zr_6O_4(OH)_4(carboxylate)_{12}$ secondary building units (Figure 2). In general, most of the Zr-based MOFs i) are stable in boiling water and heating in air to 350°C; ii) decompose above 500°C; iii) are resistant to most chemicals, including acids, bases with high radiation stability; and iv) retain crystallinity even after exposure to 10 ton/cm^2 of external pressure. The high degree of network connectivity is believed to be the main reason for the high stability of Zr-based MOFs compared to other MOFs.

Although MOFs have been shown to be a very promising material, one fundamental issue impeding the large-scale deployment in commercial and industrial applications is the high pulverulent properties. As part of this, as-obtained CuBTC and synthesized (UiO-67) MOF powders were converted into engineered beads using the wet granulation approach utilizing poly methyl methacrylate (PMMA). We selected PMMA as a binder because it is structurally flexible, transparent, ultraviolet tolerant, as well as chemically and heat resistant.

2.0 SYNTHESIS AND CHARACTERIZATION OF CUBTC and UIO-67

The CuBTC MOF was purchased from Aldrich chemicals, sold under the name Basolite C 300, and directly used to fabricate engineered composites. The synthesis of UIO-67 was adapted from a previously reported method.[11] In 50 mL of dimethylformamide, 2.5 mmol of $ZrCl_4$ and 2.5 mmol of biphenyldicarboxylic acid were stirred before the addition of 1.43 mL of acetic acid and 100 mL of HCl (Teflon liner). The Teflon liner containing the mixture was inserted in a Parr vessel which was placed in an oven at 120°C for 24 hours. After cooling to room temperature, the mixture was filtered using Buchner funnel to collect the solid products. The solids were subsequently washed with dimethylformamide and acetone. The remaining solids were collected and placed in an oven at 90°C to dry overnight. Both CuBTC and UiO-67 powder samples were analyzed using scanning electron microscopy (SEM) to investigate the morphology and microstructures of the as-obtained and synthesized MOF powder samples. Samples were mounted onto carbon tape to observe the outer surfaces of the particles. Additionally, samples were mounted in epoxy and cross-section polished to observe the interiors of the particles (for engineered particles). All samples were sputter-coated with 20 nm of iridium to avoid sample charging under the electron beam in the microscope.

Samples were imaged with a JEOL 8530 HYPERPROBE, made by JEOL USA (Peabody, MA). The microprobe images were collected at an accelerating voltage of 30 kV, a beam current of 1 nA, and a working distance of 10.8 mm. Images were collected using the JEOL solid-state backscattered electron imaging detector. As clearly seen in Figure 3, the as-obtained CuBTC MOF has a smooth and bright surface with a wide distribution of sizes, with an average particle size of around 20 µm. The CuBTC MOF particles show the crystal shape was octahedral with triangle crystal faces clearly visible in the SEM image. On the other hand, the SEM images of UiO-67 were not as clear as the CuBTC.

Subsequently, both MOF powders were analyzed using powder X-ray diffraction (PXRD) and Brunauer-Emmett-Teller (BET) specific surface area analysis to demonstrate the purities and porosities of the as-obtained and synthesized MOFs, respectively. The MOF samples were ground to a fine powder with an agate mortar and pestle, suspended in ethanol, and pipetted onto a zero-background holder (off-axis silicon wafer). PXRD patterns were collected using a Bruker D8 Advance diffractometer equipped with a Cu-target at power settings of 40 mA and 40 kV. The goniometer was configured with a radius of 250 mm, 0.3° fixed divergent slits, 2.5° primary and secondary soller slits, and a LynxEye™ position-sensitive detector with a collection window of 3° 2θ, with the LynxEye iris set to 8 mm. Scan parameters were 0–40° 2θ with a step of 0.015° 2θ and a 0.6-second dwell at each step. The scans were collected in lock-coupled mode where the tube and detector were stepped together at equal angles through the scan range. The instrument alignment was verified to be within the manufacturer's specifications (±0.01° 2θ peak position and ±10% intensity from 5 to 125° 2θ) by scanning a NIST 1976A instrument standard prior to data collection.

As shown in Figure 4, the PXRD of the MOF powders matches well with simulated PXRD, indicating the long-range order and purity of the synthesized MOFs. To analyze the porosity of the MOF powders, BET measurements were performed on powder samples at 77 K using nitrogen as a carrier gas (Figure 5). The BET results show that the CuBTC MOF has a specific surface area of 1536 m^2/g and the UiO-67 MOF has a specific surface area of 1236 m^2/g, both of which are in the ranges of reported values. Similarly, BET specific surface area

measurements were performed under identical conditions for three carbon materials, which all had reasonable values ranging from 875 to 950 m^2/g.

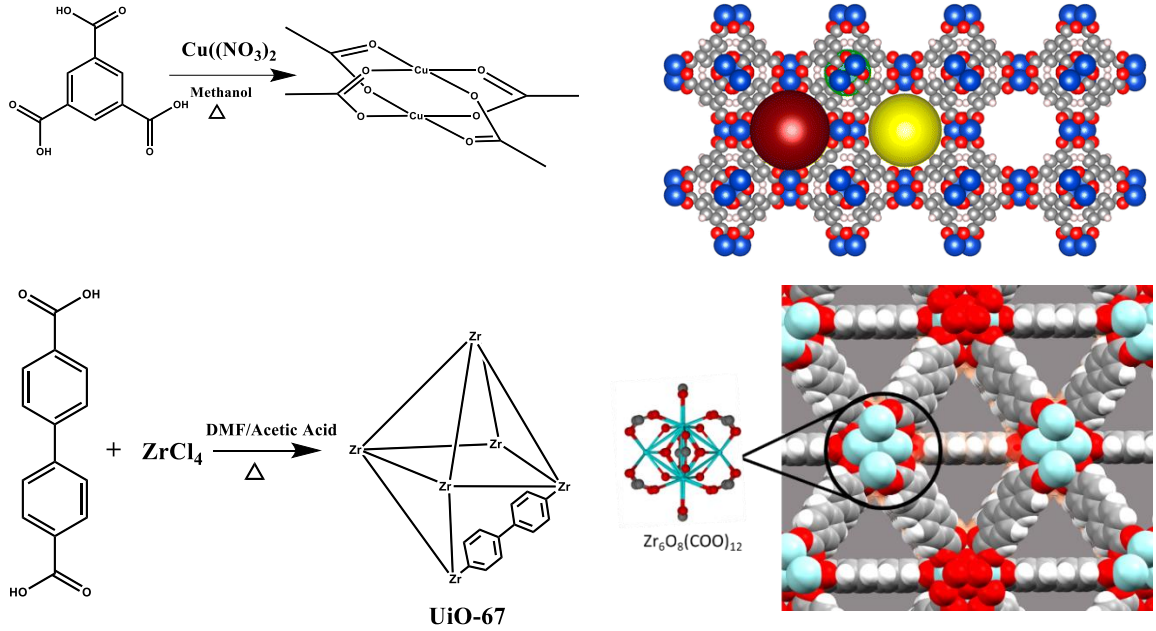

Figure 2. Schematic diagram of CuBTC (top) and UIO-67 (bottom) MOFs and corresponding three-dimensional crystal structures. Notice each Zr is connected to 12 organic building units.

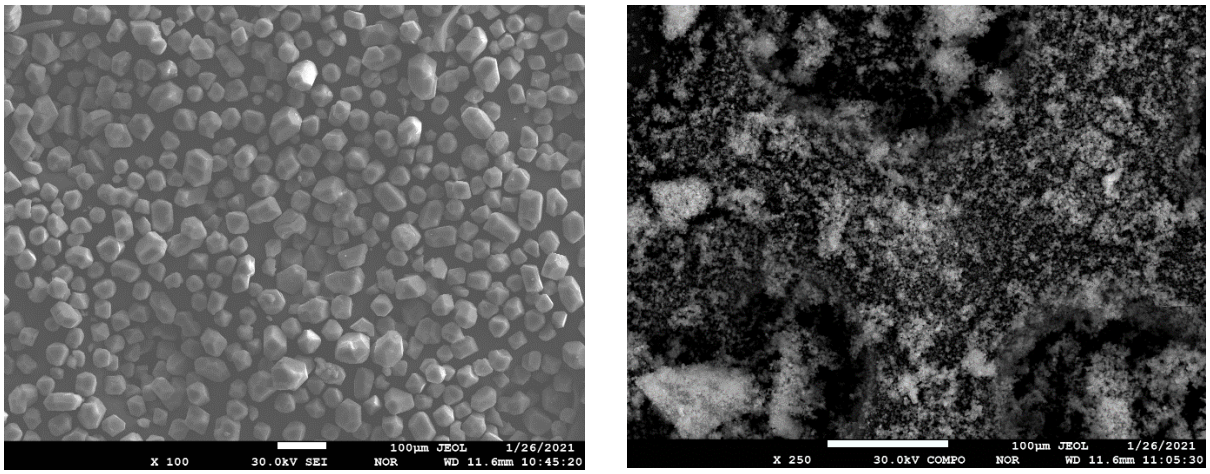

Figure 3. SEM photographs of CuBTC (left) and UiO-67 (right) MOFs showing the well-faceted, octahedral CuBTC particles with smooth and bright surfaces.

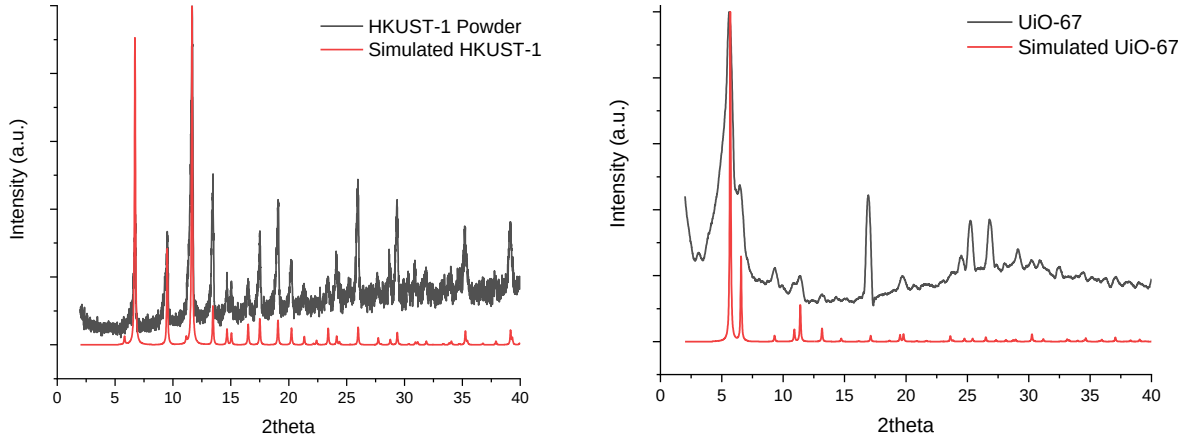

Figure 4. Simulated and experiments power X-ray diffractions of CuBTC (HKUST-1) and UiO-67. Both MOFs show identical structure with long-range order.

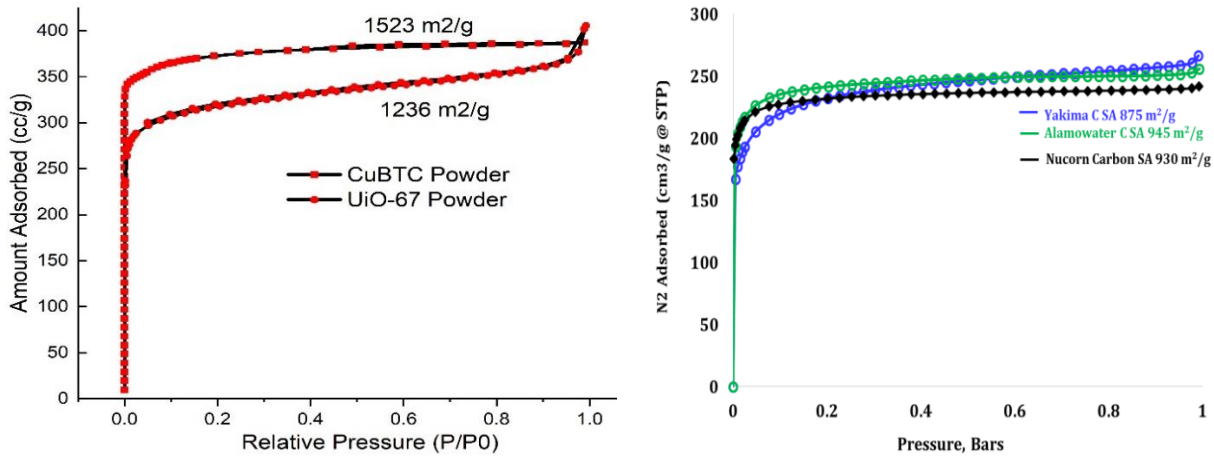

Figure 5. BET surface areas of MOF powders (left) and activated carbons (right) under identical conditions. As shown, both MOF powders tend to have double the surface area compared to the carbons tested.

2.1 FABRICATION OF CUBTC and UIO-67 INTO COMPOSITES

The commercially available (CuBTC) and synthesized (UiO-67) MOFs were converted into engineered beads using wet granulation methods as described in greater detail in an earlier report.[13] In brief, the wet granulation method was used to produce mechanically robust composites for another MOF that was studied extensively under the DOE Material Recovery and Waste Form Development Campaign. Wet granulation is a conventional method where granules are formed by adding a liquid onto a powder bed undergoing agitation. The primary powder combines with a binder material to produce a wet material that, once dried, forms robust particles. The granulation liquid can be any volatile liquid. Typical liquids include water, organic solvents, or a combination thereof. Although aqueous solutions have the advantage of being cheaper, the choice of granulation liquid depends on the inherent chemical stability of the MOF and the solubility of the binder in the granulation liquid. Importantly, this method of granulation has been demonstrated to be extremely scalable, with manufacturers of polyacrylonitrile (PAN)-

type granulators reporting tons of granules (mostly fertilizers and pharmaceuticals) being produced per hour.

Fabrication of the MOF pellets was achieved as follows. First, a known amount of PMMA (~5 wt%) and CuBTC or UiO-67 powder were sonicated in dichloromethane to solubilize the polymer and disperse the MOF powder. Dichloromethane was chosen because of its volatility and ability of dissolve PMMA. The dispersed MOF was added to a custom-built, small, pan-type granulator. During the mixing process, dichloromethane evaporated, and the resulting paste was agitated to achieve the desired particle growth. Granules with a wide size distribution were produced and sieved to obtain desired size ranges of 250 μm < x < 425 μm, 600 μm <x < 850 μm, and 1000 μm < x < 1180 μm. The particles were dried at 100°C for 12 hours in a vacuum oven. SEM, PXRD, and BET experiments were performed and compared with powder samples.

2.2 STRUCTURE VERIFICATION AND INTEGRITY

The synthesized engineered composites were analyzed using various techniques to provide structural integrity. The PXRD patterns for the synthesized and engineered composites of UiO-67 and CuBTC were taken and compared to synthesized powder samples to ensure that the engineered composites did not lose structural integrity during the fabrication and retained long-range order after pelletizing. Figure 6 and Figure 7 show PXRD and SEM patterns, respectively, in comparison with freshly synthesized MOF powders; the XRD patterns clearly match well with powder samples and simulated patterns, indicating the retention of crystallinity and long-range order of the original MOFs in the engineered particles (Figure 6).

To evaluate the morphology of the composites, SEM analysis was performed as described earlier (Figure 7). The composites were mounted in resin and cross-sectioned or cut with a razor as needed. For the beads that were cut in half with a razor blade, the halves were mounted either cut side up or cut side down on top of carbon tape on aluminum stubs. As shown in Figure 6, the CuBTC composite retained its octahedral shape and size during the fabrication process; however, all the particles were glued together as opposed to the uniform distribution as seen in the powder sample (Figure 3). This could be due to the polymer holding the particles together tightly. On the other hand, as observed for the UiO-67 powder sample, the UiO-67 composites did not show any clear particle sizes or shapes. The cross-sectional images of the composites suggest that the composite particles show some porosity. However, the morphology of the UiO-67 composite is not clearly evident under the conditions we tested. To evaluate the specific surface areas of the composite particles, the BET specific surface area measurements were performed at 77K using N_2 gas (Figure 8). The specific surface area measurements show slightly reduced values compared to powder samples, which was expected. The specific surface areas of the CuBTC and UiO-67 composites were found to be 924 and 561 m^2/g, respectively. The BET surface areas of the two MOF composites were close to carbon materials we tested (875 to 950 m^2/g).

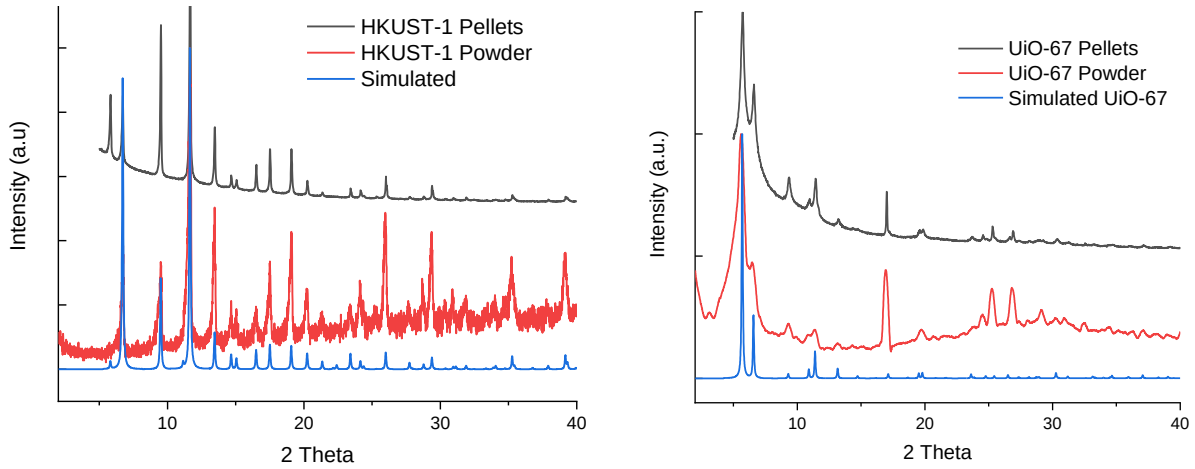

Figure 6. Simulated and experimental powder X-ray diffractions of CuBTC (HKUST-1) and UiO-67 powder and composites (PMMA). The MOF composites retain their structural integrity during the fabrication process with long-range order.

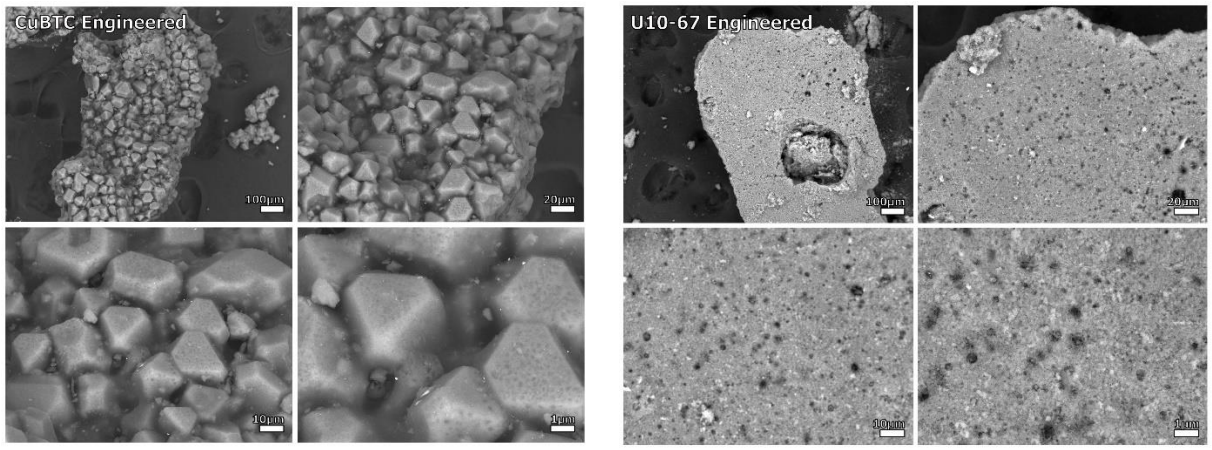

Figure 7. SEM photographs of CuBTC (left) and UiO-67 (right) composites. Well-faceted, octahedral CuBTC particles with smooth and bright surface were retained during the wet granulation process; however, all the particles were glued to polymer (left). The cross section of the UiO-67 composite is shown on the right.

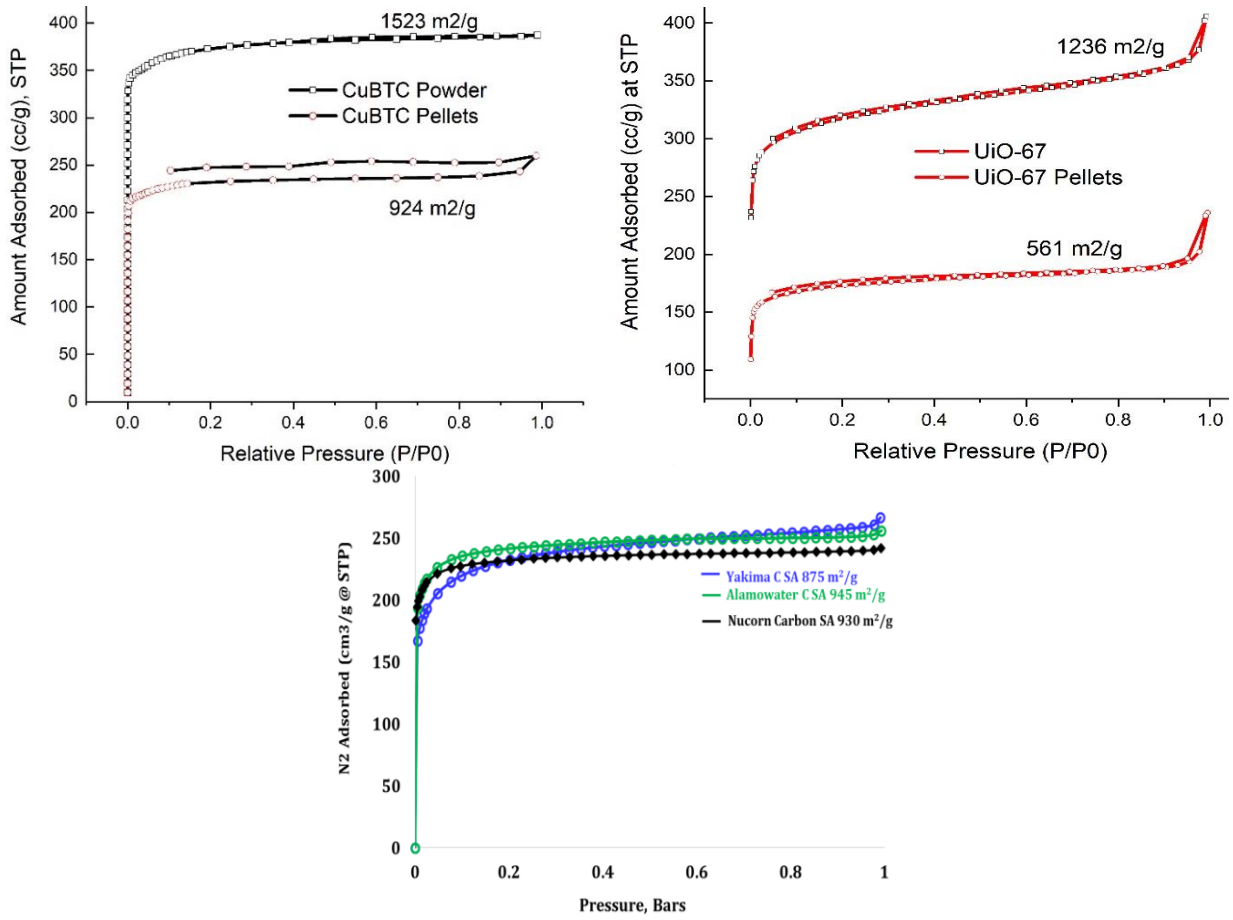

Figure 8. The BET surface areas of the CuBTC and UiO-67 composites in comparison with MOF powder and activated carbons.

2.3 EVALUATING MECHANICAL STABILITY

In addition to PXRD, the composite particles were tested for mechanical stability using a shaker table to determine how well the pellets retained their size and shape. In this experiment, the pellets of the MOF were placed in a 20-mL scintillation vial and strapped in a shaker table. The table was then shaken at 200 rpm for 20 minutes, then for 40 minutes, and then repeated at 400 rpm. At the end of each time interval, the contents of the vials were passed through the sieve of their respective sizes and the collected pellets were massed and compared to the initial mass of the pellets to determine the amount powderized from the test. The data from this experiment is given in Table 1. From the table, the smaller pellet sizes retained their pellet forms more than their larger counterparts, which suggests that they are more mechanically stable. We

expect the mechanical stability of the UiO-67 PMMA composites would be the same as that of the CuBTC PMMA composites.

Table 1. Mechanical stability evaluation of CuBTC composites using shaker table.

CuBTC Composite	250 μm < x <425 μm (% powderized)	600 μm < x < 850 μm (% powderized)	1000 μm < x < 1180 μm (% powderized)
20 min @ 200 rpm	0.55	1.25	1.01
40 min @ 200 rpm	0.56	0.89	1.24
20 min @ 400 rpm	2.78	3.72	10.9
40 min @ 400 rpm	1.58	2.61	8.17
Cumulative loss	5.37	8.23	20

2.4 XENON AND KRYPTON GAS ADSORPTION

Single-component gas adsorption experiments involving krypton and xenon were performed on the CuBTC and UiO-67 powders and composites sized from 600 mm to 825 mm using a Quantachrome adsorption instrument. Prior to gas adsorption, MOF powder and composites were activated at high temperature and under vacuum to remove any trace amount of solvent or air. Both the CuBTC and the UiO-67 powders and pellets were initially activated at 150°C under vacuum for 12 hours; however, under these activation conditions, the powder samples displayed a Xe uptake much lower than previously obtained.[14] The activation condition was thus changed to 180°C for the powder samples, though the same could not be done for the pellets as the melting temperature for PMMA is 160°C. This limitation on the activation could inhibit the pellets from making full use of the total capacity of the incorporated MOFs.

After activating the powder samples, the single-component gas experiments were run at the temperatures of 193 K, 233 K, 253 K, 278 K, and 298 K from a low relative pressure of P/P_0 of 0.005 to 760 mm Hg (P_0 = 760 mm Hg) (some of the data removed from this report for clarity). These adsorption and desorption isotherms are shown in Figure 9. The CuBTC powder shows steep uptake at relatively low pressure (<0.1 bar), which is of interest to many nuclear applications because noble gases are present at relatively low concentrations (~1000 ppm) in molten salt reactors and nuclear reprocessing plants. The CuBTC powder has approximately 14 mmol of Xe per gram of material at 193 K, twice that of UiO-67 powder (6 mmol/g); however, at low pressure (<0.1 bar) CuBTC powder has approximately seven times the capacity of the UiO-67 powder. The steep Xe uptake indicates that CuBTC would adsorb Xe quite readily at lower concentration, making it ideal for separating Xe from an off-gas stream. The steep uptake in CuBTC can only be explained by the presence of unsaturated metal sites along with a higher specific surface area; however, the Xe adsorption in CuBTC powder was slightly lower than the reported value (18 mmol/g). This could be due to improper activation or the presence of defects in the previously reported sample. It has been widely documented that defects tend to improve the gas adsorption in MOFs.

The adsorption data clearly demonstrates that the CuBTC powder outperforms the UiO-67 powder in terms of Xe loading at 193K, but neither sorbent has any reasonable capacity at room temperature. The Kr adsorption and desorption data are plotted in Figure 9 for both the CuBTC and UiO-67 powder; the poor uptake shown suggests the higher selectivity toward Xe over Kr at 193 K and room temperature.

Like the powder samples, the CuBTC and UIO-67 (PMMA) composites were evaluated toward Xe and Kr adsorption and desorption under identical conditions. As indicated earlier, prior to adsorption, both composite materials were activated at 150°C for 12 hours due to the lower melting point of PMMA as opposed to activating at 180°C or higher. The Xe and Kr adsorption and desorption plots of the composites are shown in Figure 9. The CuBTC (PMMA) composite has a 50% reduction in Xe loading at 193 K and pressure 0 to 1 bar. A similar trend was observed for the UiO-67 (PMMA) composite. On the other hand, both composites have reduced Kr capacity, but the reduction is not as pronounced as it is for Xe. The 50% reduction in Xe loading might be strongly correlated to the lower activation temperatures used for the CuBTC (PMMA) composites because of lower melting point of PMMA. The PXRD, SEM, and BET experiments of the composite show identical morphology and porosity compared to powder sample so the possibility of structural degradation can be ruled out. As opposed to CuBTC PMMA composites, we recently reported CuBTC composites with varying amounts (0 to 90%) of PAN as a polymer binder.[14] The CuBTC PAN composite (90% CuBTC and 10% PAN) is shown to have 16 mmol/g of Xe at 193 K, higher than CuBTC powder and CuBTC PMMA composite under identical conditions. The CuBTC PAN composites were also activated at same temperature (150°C) as the CuBTC PMMA composites.

Several possibilities for the reduced Xe loading in the CuBTC (PMMA) composites are studied here: i) the vacuum being pulled during activation is not as strong, so it would be an instrumental error; ii) because of the lower melting point of PMMA, the PMMA might have diffused inside the MOF pore space and blocked the pores; iii) the polymer incorporation between the two methods is fundamentally different, as the wet granulation method virtually glues CuBTC together whereas the MOF (PAN) composite method seems to form a polymer shell with the MOF inside; and/or iv) PAN is highly polar whereas PMMA is not. The change in polarity from the polymer could impact interactions between the polymer/MOF interface, which might lead to a reduction in capacity. These hypotheses will need to be evaluated to understand the reduction in noble gas adsorption in the CuBTC and UiO-67 (PMMA) composites.

The data collected from the CuBTC powder and composites (PMMA and PAN) were also compared with activated carbon at 193 K. As shown in Figure 9, the Xe adsorption for the CuBTC PAN (90%HK) composite has exceptional performance compared to activated carbons; we expect similar or higher performance toward CuBTC PMMA composites, but more experiments are needed to resolve the issues identified above.

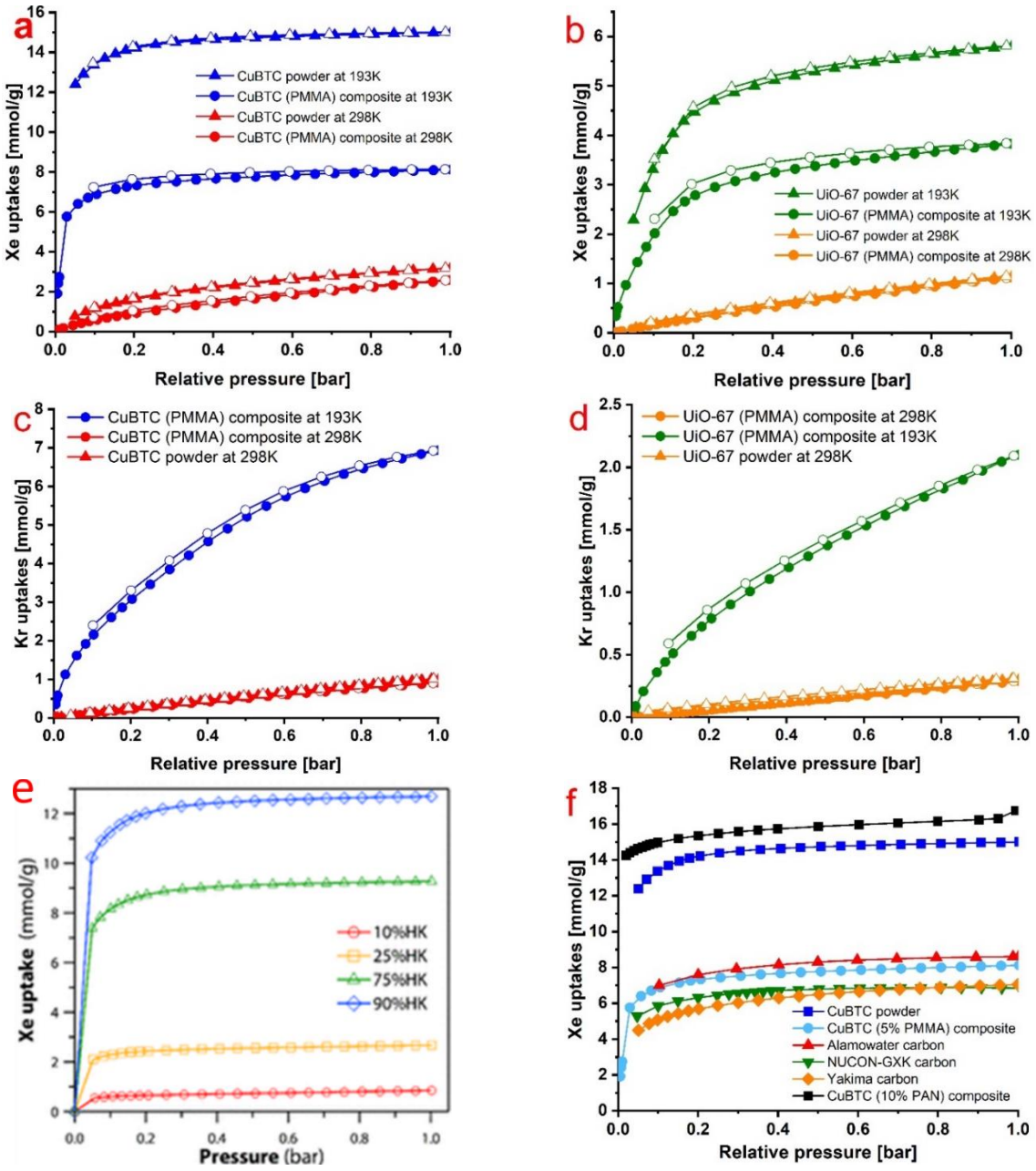

Figure 9. The Xe and Kr adsorption of MOF powders and composites in comparison with activated carbon performed at room temperature and 193K from 0 to 1 bar pressure: a) Xe adsorption in the CuBTC powder and composite (PMMA) at room temperature (RT) and 193 K; b) Xe adsorption in the UiO-67 powder and composite (PMMA) at RT and 193 K; c) Kr adsorption in the CuBTC powder and composite (PMMA) at RT and 193 K; d) Kr adsorption in the UiO-67 powder and composite (PMMA) at RT and 193 K; e) Xe loading at 193 K in the CuBTC PAN composites (with varying amounts of PAN) – as shown, the 90%HK sample (90% CuBTC and 10% PAN) has the highest Xe loading at 193 K; and f) comparison of CuBTC powder and composites (PMMA and PAN) with activated carbons at 193 K.

3.0 RADIATION STABILITY

After successful fabrication of MOF composites, gamma radiation (Co-60) experiments were performed at PNNL. In order to reduce the irradiation duration (and therefore cost), a source distance was selected that resulted in the highest dose rate possible while allowing all 12 samples to be irradiated together to a uniform dose rate. The distance targeted was 7.0 cm from source center to sample center. To accommodate this, a thin wire mesh was bent to a radius of approximately 7.0 cm and taped to the irradiation port at the ~7-cm distance. Using a calibrated micro-volume ionization chamber, the dose rate was measured at various positions along the grid surface (and at the distance from the grid surface estimated to be where the powder volumes would be centered) to ensure a uniform dose rate, and was found to be 15.5 kGy/hr in terms of air kerma (16.9 kGy/hr in terms of absorbed dose to water). The actual source-to-powder center distance ended up at ~6.9 cm.

Table 2. Radiation dose rate and time required to achieve 1000 kGy radiation for CuBTC and UiO-67 powder and engineered particles.

Run	MOF	kGy/hr	kGy	Time (hr)
1	CuBTC and UiO-67 powder and PMMA composite (600 mm size)	**10**	**200**	**20**
2	CuBTC and UiO-67 powder and PMMA composite (600 mm size)	**10**	**500**	**50**
3	CuBTC and UiO-67 powder and PMMA composite (600 mm size)	**10**	**1000**	**100**

The 12 small glass vials provided were divided into three sets (indicated by the labels “1,” “2,” and “3” in **Error! Reference source not found.**), with each set consisting of the four different p owders and engineered beads. Each set of four vials was taped together with scotch tape at a curvature that matched the curved wire mesh, then each set was taped to the wire mesh – the three sets together centered in the Co-60 field (Figure 10). The Co-60 source (~7900 curies) was then exposed for 13.33 hours, after which the first samples set was removed, an additional 20.0 hours before the second set of samples was removed, then an additional 33.33 hours before the last set was removed. The resulting doses to the three sets were 200, 500, and 1000 kGy in terms of air kerma (218, 546, and 1092 kGy in terms of absorbed dose to water). The associated uncertainty in the delivered doses to sample center is estimated to be ~8% at the 95% confidence level. The characterization of the irradiated samples is under investigation and will be reported in next milestone.

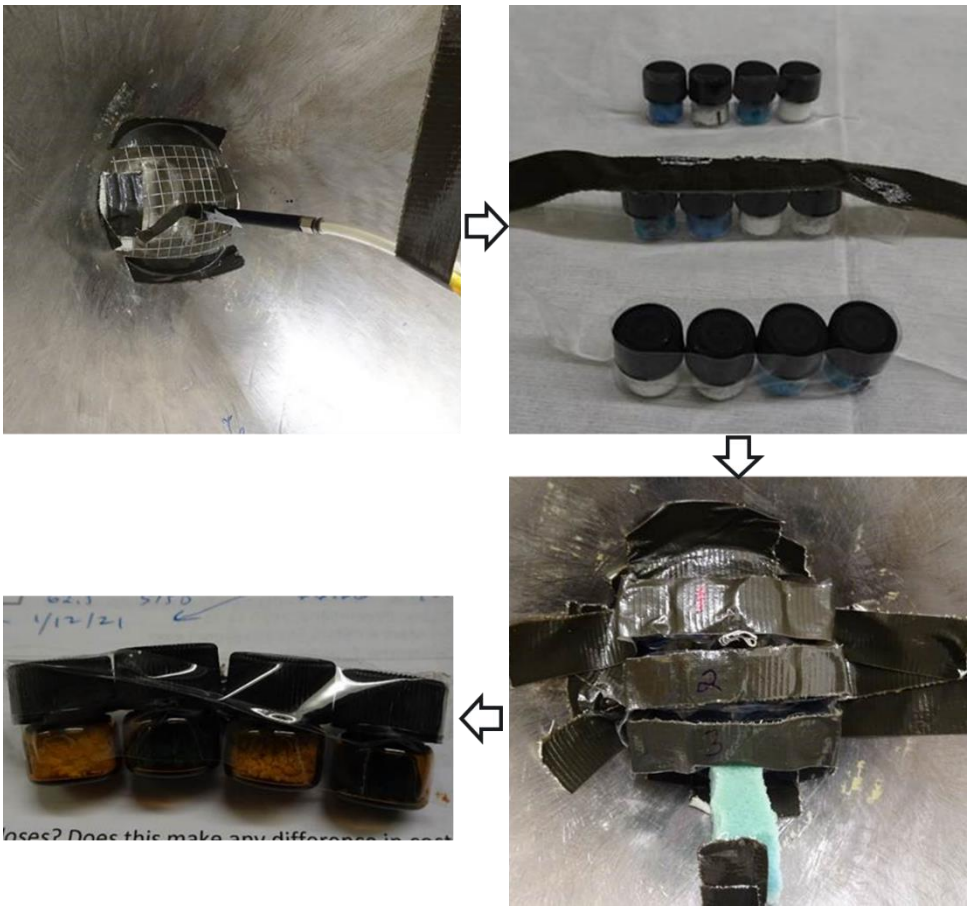

Figure 10. Clockwise: Mesh curved to a 7-cm radius and secured to the 70° beam port. Small device shown is the micro-volume ionization chamber to calibrate the Co-60 gamma-ray field at various locations on the grid, each of the three groups (1, 2, and 3, see Error! Reference s ource not found.) secured together with tape for preparation for irradiation geometry. Each sample set secured with tape to the surface of the curved mesh. The resulting distance from center of powder for each vial to center of Co-60 source is 6.9 cm, and measured to be 15.5 kGy/hr air kerma rate and sample set #1 after its irradiation was completed and calculated to be 206 kGy ± 8% at the 95% confidence level. Note browning of glass from the high dose.

3.1 CHARACTERIZATION OF POST IRRADIATED MOFs

Irradiated MOF powder and composites were characterized using various analytical techniques, including PXRD, SEM, mechanical stability, BET specific surface area analysis, and noble gas adsorption at low temperature, to make sure all the MOFs retained their structural integrity after gamma radiation exposure. Given the large number of samples exposed to radiation, we are characterizing MOFs exposed to the highest radiation (1000 kGy).

3.1.1 MECHANICAL STABILITY TESTING

Similarly, for the as-synthesized MOF composites given in Table 1, mechanical stability tests of MOF composites exposed to radiation were performed using shaker table. In this test, the radiated pellets were put into vials which were then placed securely on a shaker table, shaken at 200 rpm for 20 minutes, then 40 minutes, before being shaken at 400 rpm for 20 minutes and then for an additional 40 minutes. The material was passed through a sieve after each test and the remaining pellets were massed to obtain the amount of mass lost due to powderization of the pellets from the shaker table test. Compared to our previous mechanical stability tests with pelletized MOFs, we changed the container size to be smaller, thus giving less free space. This change was made to allow for more agitation of the samples as this will limit the space within which the pellets could move freely.

The results of this experiment are given in Table 3. The data in the table shows that there are no clear trends between radiation dosage and powderization of the pellets. The sample that had the lowest degree of powderization was the sample that was irradiated with 500 kGy instead of the sample that received the lowest dosage of 200 kGy. This result shows that the powderization of the samples cannot be attributed fully to the dosage of radiation received and differences in powderization could be attributed to another variable such as position on the shaker table. These results are promising as they indicate that radiation exposure may not compromise the integrity of the pellets; however, maintaining the integrity of the pellets may not necessarily mean that the crystal structure of the MOFs is maintained after exposure. To test whether the MOFs retained their structures, PXRD and SEM measurements were performed.

Table 3. Mechanical stability of MOF composites after radiation exposure

	200 kGy		500 kGy		1000 kGy	
	CuBTC	UiO-67	CuBTC	UiO-67	CuBTC	UiO-67
	%Powderized	%Powderized	%Powderized	%Powderized	%Powderized	%Powderized
20 min @ 200 rpm	11.16	2.03	7.09	5.42	13.54	5.26
40 min @ 200 rpm	7.93	4.75	2.82	2.49	3.54	6.08
20 min @ 400 rpm	0.44	7.68	2.73	5.93	6.67	6.7
40 min @ 400 rpm	6.44	7.69	3.1	5.01	9.21	8.83
Cumulative Loss	23.82	20.47	14.89	17.59	29.34	24.3

3.1.2 STRUCTURAL INTEGRITY OF IRRADIATED MOFS

To check the structural integrity of the irradiated MOFs, PXRD measurements were taken on the irradiated samples and compared with the PXRD results for their unirradiated counterparts. As shown in Figure 11, the CuBTC and UiO-67 powders and composites appear to maintain their structural integrity even after exposure to 1000 kGy radiation. All the major peaks remained present in both irradiated CuBTC and UiO-67 powders and composites, showing that the crystal structure remains mostly intact; however, subtle differences were observed. The UiO-67 composite shows drastic changes in the diffraction pattern after irradiation. The peak around 5° 2θ broadened significantly and nearby peaks could not be resolved. This broadening of peaks in the UiO-67 composite is most likely due to

the presence of PMMA, as this phenomenon is not observed for the powder sample. We believe this may be due to the lower melting temperature of the PMMA, which might be evaporating and starting to fill pores of the UiO-67; however, the CuBTC composite does not show any peak broadening. To see if there are any changes in morphology of the irradiated particles, SEM was performed as described earlier.

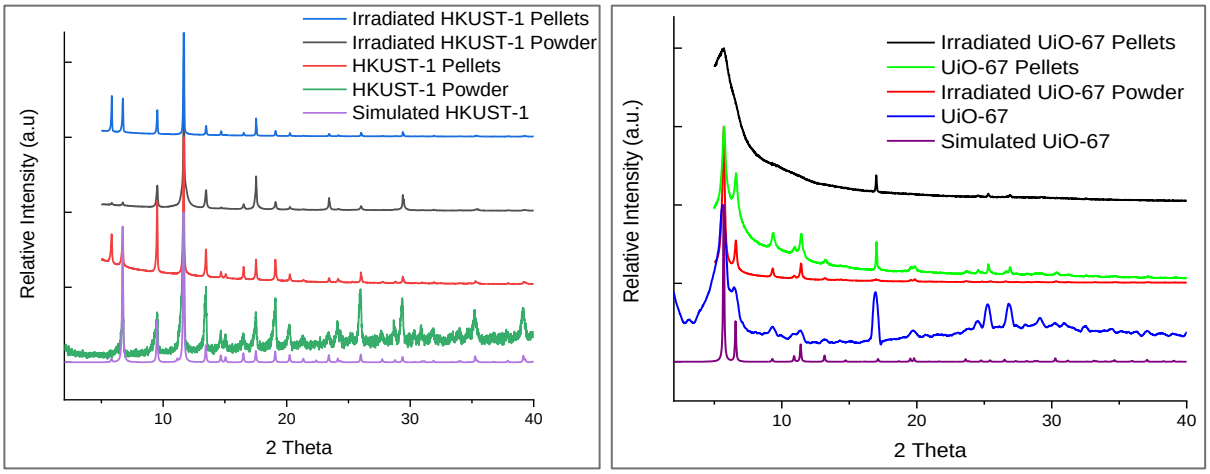

Figure 11. PXRD plots of irradiated CuBTC (left) and UiO-67 (right) powders and composites with their unirradiated counterparts.

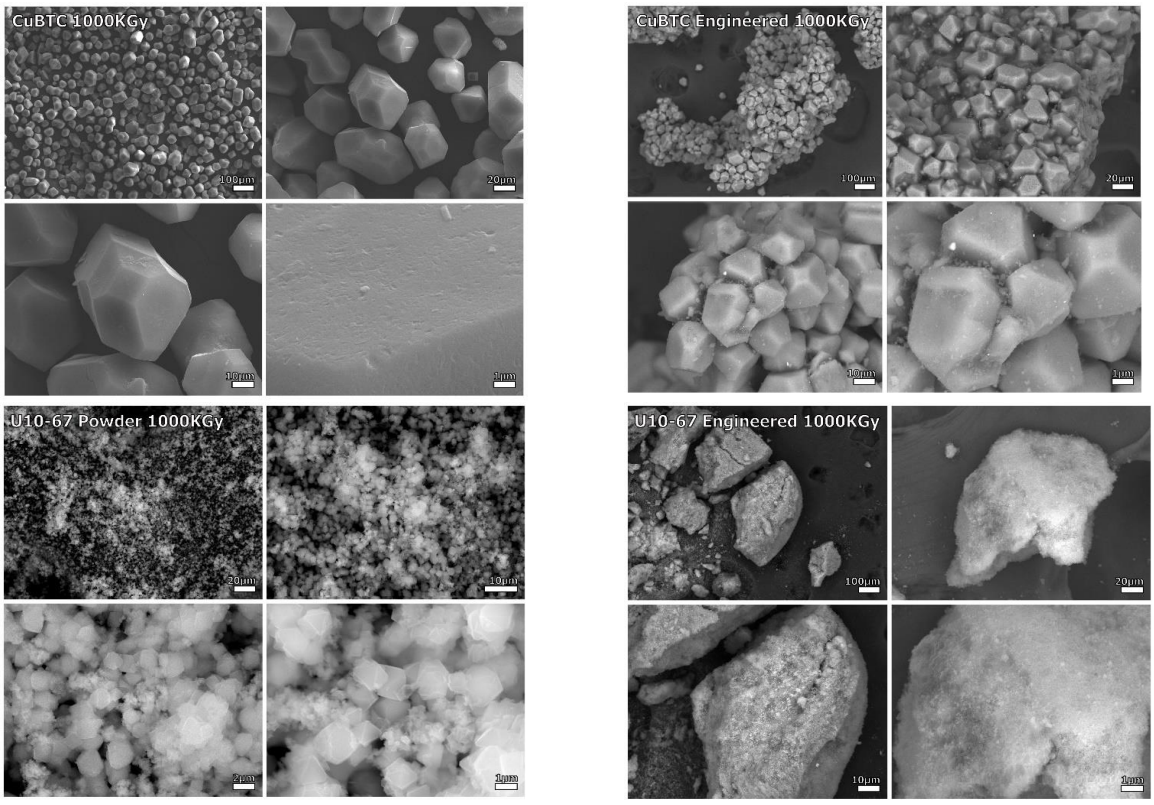

Figure 12. SEM images of the irradiated (1000 kGy) (top) CuBTC and (bottom) UiO-67 (left) powder and (right) composites.

As shown in Figure 12, irradiated the CuBTC powder and composite show octahedral shape with a wide size distribution of the particles. The irradiated CuBTC composite particles were similar to the unirradiated CuBTC composite, where the octahedrally shaped particles were agglomerated together; however, higher magnification of the CuBTC composite indicates that distribution of small particles within the larger MOF particles could be resulting from the polymer. The irradiated UiO-67 powder shows irregularly shaped crystals at higher magnification and was clearly visible, while the UiO-67 composite lacks clear distinction of shaped crystal, which is similar to UiO-67 composite before irradiation as shown in Figure 7.

3.1.3 BET SURFACE AREA OF IRRADIATED MOFS

To further understand the impact that radiation had on the adsorption properties of the MOFs, BET specific surface area analysis was conducted. In gas adsorption experiments, the irradiated samples were activated to remove anything that might have adsorbed onto the material due to exposure to the ambient atmosphere, namely water and CO_2. After activation, the samples were put into sample analysis ports on the instrument and placed into baths to control the temperature of the analysis. To collect the isotherm, the instrument releases a known volume of gas into the samples and measures the pressure after releasing that gas. By defining equilibrium pressures, the instrument will release known amounts of gas until that equilibrium pressure is achieved. The difference between the amount of gas needed to reach that pressure and the actual amount of gas used to reach that pressure is the amount of gas that the sample adsorbed. The BET method uses the amount of gas adsorbed, primarily with nitrogen at 77 K, to estimate the surface area of the material. The instrument used for these experiments was the Quantachrome Autosorb IQ_2 instrument.

Table 4. **BET surface area of MOF composites after irradiation in comparison with MOF powder and composites before irradiation**

Material	Surface Area (m^2/g)
CuBTC powder before irradiation	1523
CuBTC composite before irradiation	924
CuBTC composite after irradiation (1000 kGy)	901
UiO-67 powder before irradiation	1236
UiO-67 composite before irradiation	561
UiO-67 composite after irradiation (1000 kGy)	20

The results from the BET specific surface area analysis are given in Table 4. As seen in the table, the difference in specific surface area for the irradiated CuBTC composite was minimal and well within measurement error, further indicating the porosity. The results for the UiO-67 composite, however, showed drastically different results. We noticed a decrease in specific surface area from 561 to 20 m^2/g. This would corroborate the hypothesis that the PMMA polymer filled the pores upon exposure to radiation for the UiO-67 composite. Further experiments are underway to evaluate the irradiated composite material for noble gas adsorption.

4.0 CONCLUSIONS

In conclusion, we synthesized, characterized, and fabricated mechanically robust engineered particles of MOFs using the wet granulation approach with PMMA as a polymeric binder. Further, 12 MOF powders and engineered beads were exposed to Co-60 gamma radiation to achieve a total radiation dose of 1000 kGy. The noble gas adsorption experiments were performed on MOF powder and composites and compared with activated charcoal at 193 K between 0 to 1 bar pressure (irradiated sample characterization is underway). The MOF powder was shown to have double the Xe loading compared to charcoal, whereas MOF (PMMA) composites showed 50% reduction in noble gas adsorption compared with MOF powder.

The Xe loading in MOF PMMA composite is contracting with our previously reported MOF (PAN) composite even though we used an identical activation procedure. We hypothesized that the reduction in Xe loading in MOF PMMA composite could be i) the vacuum being pulled during activation is not as strong (i.e., instrument error); ii) the polymer incorporation between the two methods is fundamentally different as the wet granulation method virtually glues CuBTC together whereas the MOF (PAN) composite method seems to form a polymer shell with the MOF inside; or iii) PAN is highly polar whereas PMMA is not. The change in polarity from the polymer could impact interactions between polymer/MOF interface that might lead to reduction in capacity. These hypotheses will need to be evaluated to understand the reduction in noble gas adsorption in CuBTC and UiO-67 (PMMA) composites going forward.

5.0 References

1. Banerjee, D.; Simon, C. M.; Elsaidi, S. K.; Haranczyk, M.; Thallapally, P. K., Xenon Gas Separation and Storage Using Metal-Organic Frameworks. *Chem-Us* **2018,** *4* (3), 466-494.
2. Banerjee, D.; Cairns, A. J.; Liu, J.; Motkuri, R. K.; Nune, S. K.; Fernandez, C. A.; Krishna, R.; Strachan, D. M.; Thallapally, P. K., Potential of Metal-Organic Frameworks for Separation of Xenon and Krypton. *Accounts Chem Res* **2015,** *48* (2), 211-219.
3. Soelberg, N. R.; Garn, T. G.; Greenhalgh, M. R.; Law, J. D.; Jubin, R.; Strachan, D. M.; Thallapally, P. K., Radioactive Iodine and Krypton Control for Nuclear Fuel Reprocessing Facilities. *Sci Technol Nucl Ins* **2013,** *2013*.
4. Ladshaw, A. P.; Wiechert, A. I.; Welty, A. K.; Lyon, K. L.; Law, J. D.; Jubin, R. T.; Tsouris, C.; Yiacoumi, S., Adsorbents and adsorption models for capture of Kr and Xe gas mixtures in fixed-bed columns. *Chem Eng J* **2019,** *375*.
5. Banerjee, D.; Simon, C. M.; Plonka, A. M.; Motkuri, R. K.; Liu, J.; Chen, X. Y.; Smit, B.; Parise, J. B.; Haranczyk, M.; Thallapally, P. K., Metal-organic framework with optimally selective xenon adsorption and separation. *Nature Communications* **2016,** *7*.
6. Liu, J.; Fernandez, C. A.; Martin, P. F.; Thallapally, P. K.; Strachan, D. M., A Two-Column Method for the Separation of Kr and Xe from Process Off-Gases. *Ind Eng Chem Res* **2014,** *53* (32), 12893-12899.
7. Elsaidi, S. K.; Ongari, D.; Xu, W. Q.; Mohamed, M. H.; Haranczyk, M.; Thallapally, P. K., Xenon Recovery at Room Temperature using Metal-Organic Frameworks. *Chem-Eur J* **2017,** *23* (45), 10758-10762.
8. Riley, B. J.; McFarlane, J.; DelCul, G. D.; Vienna, J. D.; Contescu, C. I.; Forsberg, C. W., Molten salt reactor waste and effluent management strategies: A review. *Nucl Eng Des* **2019,** *345*, 94-109.
9. P., N. J. *Status of noble gas removal and disposal report*; Oak Ridge National Laboratory, ORNL-TM-3515: 1971.
10. Elsaidi, S. K.; Ongari, D.; Mohamed, M. H.; Xu, W. Q.; Motkuri, R. K.; Haranczyk, M.; Thallapally, P. K., Metal Organic Frameworks for Xenon Storage Applications. *Acs Mater Lett* **2020,** *2* (3), 233-238.
11. Salomon, W.; Roch-Marchal, C.; Mialane, P.; Rouschmeyer, P.; Serre, C.; Haouas, M.; Taulelle, F.; Yang, S.; Ruhlmann, L.; Dolbecq, A., Immobilization of polyoxometalates in the Zr-based metal organic framework UiO-67. *Chem Commun* **2015,** *51* (14), 2972-2975.
12. Chui, S. S. Y.; Lo, S. M. F.; Charmant, J. P. H.; Orpen, A. G.; Williams, I. D., A chemically functionalizable nanoporous material [Cu-3(TMA)(2)(H2O)(3)](n). *Science* **1999,** *283* (5405), 1148-1150.
13. Thallapally, P. K., Sinnwell, M. A.. Kuang, W., Simmons, K. L. *Develop Engineered Forms of MOF with Polymers*; PNNL-28497. Richland, WA: Pacific Northwest National Laboratory.: 2019.
14. Riley, B. J.; Chong, S.; Kuang, W. B.; Varga, T.; Helal, A. S.; Galanek, M.; Li, J.; Nelson, Z. J.; Thallapally, P. K., Metal-Organic Framework-Polyacrylonitrile Composite Beads for Xenon Capture. *Acs Appl Mater Inter* **2020,** *12* (40), 45342-45350.

Pacific Northwest National Laboratory

902 Battelle Boulevard
P.O. Box 999
Richland, WA 99354
1-888-375-PNNL (7665)

www.pnnl.gov